Automated heart rate estimation in fish embryo

Élodie Puybareau, Hugues Talbot, Marc Léonard

Automated heart rate estimation in fish embryo

Elodie Puybareau[1], Hugues Talbot[1] and Marc Léonard[2]
[1] LIGM, Université Paris-Est, France
e-mail: {elodie.puybareau, hugues.talbot}@esiee.fr
[2] L'ORÉAL Research & Innovation, Aulnay sous Bois, France
e-mail: MLEONARD@rd.loreal.com

***Abstract*— Transparent organisms such as fish embryos are being increasingly used for environmental toxicology studies. These studies require estimating a number of physiological parameters. These estimations may be diverse in nature and can be a challenge to automate. Among these, an example is the development of reliable and repeatable automated assays for the determination of heart rates. To achieve this, most existing method rely on cyclical luminance variations, since as the heart fills and empties, it become respectively brighter and darker. However, sometimes direct measurement of the heart rate may be difficult, depending on the age of the embryo, its actual transparency, and its aspect under the microscope. It may be easier to seek an indirect measurement. In this article, we estimate the heart function parameters, such as heart frequency, either from measuring the heart motion or from blood flow in arteries. This measurement is more complex from the image analysis point of view, but it is more precise, more physically meaningful and easier to use in practice and to automate than measuring illumination changes. It may also be more informative. We illustrate on medaka embryos.**

***Keywords*— Stabilization, registration, frequency analysis, optical microscopy, motion analysis.**

I. Introduction

Fish embryo models are used increasingly for human disease modeling, chemical toxicology screening, drug discovery and environmental toxicology studies [1]. In many of these studies, assessing the fish embryo cardiovascular function is key to predict the potential adverse effects of chemicals at sub-lethal concentrations [2], [3]. Testing large numbers of molecules with this model at various exposure concentrations requires a fast and reliable tool able to process large amounts of data. To this end, we propose a unique, robust and automatic tool for estimating the frequency of various physiological processes from videos taken under a microscope. We illustrate this tool on medaka embryo. The Medaka (Oryzias latipes) is a commonly used fish embryo model in toxicology, ecotoxicology and developmental biology [3]. The embryonic stages of development are transparent and internal organs, such as heart and vessels, are readily visible. Manipulations such as nano and micro-injections are also easier to perform on such organisms.

In this article we study elements that exhibit cyclic behavior, such as a beating heart, or the speed of blood cells in vessels. We propose a single tool capable of analyzing these two different types of cycles. Various methods already exist for estimating frequencies based on motion: for instance tracking methods [4], [5], integrated box methods [6], measuring the amount of changing pixels between frames [7], and optical flow [8]. Tracking methods follow one or more elements of a sequence. Hence they can estimate a proper motion together with a position, and so can be used to estimate frequencies associated with variations in motion. Integrated boxes, such as linescans, measure the change of luminosity in a fixed image subset. Change of luminosity in the box over time yields a pattern associated with the motion. Variations in grey level in the box through the sequence can be used to estimate the frequency of spatial cycles. Similarly, measuring the number of changing pixels between frames is correlated to the speed of the change, under ideal conditions [7]. Optical flow is defined as the apparent motion of objects between two consecutive images.

In our case, tracking methods are in practice unusable, particularly since moving elements of interest can be difficult to identify and segment. Indeed, the appearance of moving elements may change significantly during motion, since it occurs in 3D and we only measure 2D information. We cannot use integrated box methods either because motion may not be spatially cyclic, is 3D and may not involve large illumination variations. Similarly, measuring changing pixels between frames is simple, but does not correspond to a physical measurement, is sensitive to noise and spurious motion. In contrast, optical flow can be rendered insensitive to global motion via image stabilization, is generally robust to noise and does indeed correspond to a physical measurement.

The remainder of the article is as follows: in Section 2 we present our methodology, in Section 3 we show our results. We validate in Section 4 and then conclude in Section 5.

II. Methodology

A. Experimental protocol

Medaka embryos were anaesthetized with tricaine for immobilization, placed under a Leica DMi8 inverted brightfield microscope and 600×480 2D video was acquired with a $\times 20$ objective and a $\times 10$ focusing lens, at a frame rate of 100 frames per second via a high-speed camera. The calibration was 2μm per pixel, sufficient to identify the motion of blood cells in the bloodstream. Embryos were captured at various stages of their development between 1-7 days after hatching, and exposed to various substances, some of which induced either bradycardia or tachycardia. The acquired video stream exhibit various artifacts, including noise, global motion due to vibrations, remaining embryo motion and spurious stage motion, as well as sensor pattern.

B. Frame preprocessing

In a production environment, microscopes may be difficult to stabilize and so vibrations may be present in our sequences and the embryo may still move slightly. Our acquisitions show not only the subject of study but also a fixed-grid texture-like pattern often present in high-speed sensors. After sequence stabilization, this grid would no longer be fixed and so would impair further processing. We therefore need to remove this texture beforehand. To obtain an image of this texture, we computed the average image of the unstabilized sequences, and we subtracted it from the same image on which we applied a Gaussian filter with $\sigma = 1$. This high-pass filter conserves only the high-frequency elements. This texture is then subtracted from each image of the whole sequence. This removes the grid without blurring the sequence. The result may contain other high-frequency, non-grid elements of the sequences, but these are non-moving and so do not affect the end result. This is illustrated in Fig 1.

$$\forall I \in \mathcal{S} : I_{clear} = I - \left(\bar{\mathcal{S}} - \mathcal{G}_{\sigma=1}(\bar{\mathcal{S}})\right) \tag{1}$$

with $\mathcal{G}_{\sigma=1}$ a gaussian filter with standard deviation $\sigma = 1$, $\bar{\mathcal{S}}$ is the average of the sequence $\mathcal{S}$. $\mathcal{S}_2$ is the sequence of the I_{clear}.

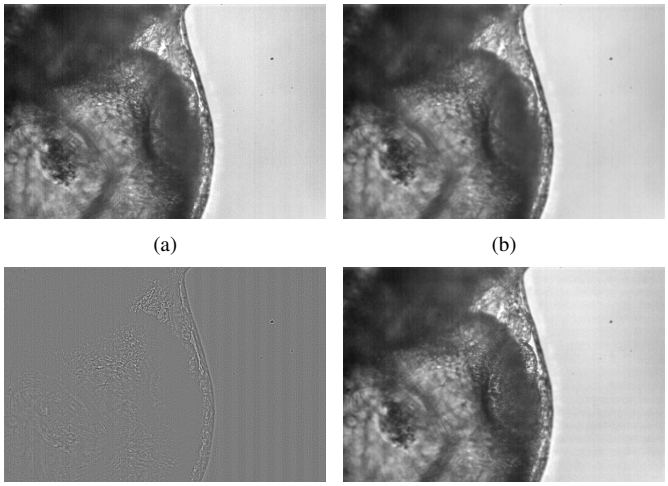

(a) (b) (c) (d)

Fig. 1. Removing sensor pattern from the acquisition. (a) The average of the sequence yields the non-moving parts of the sequence. (b) Blurred average removes thin and textured elements. Computing (a)-(b)=(c) yields the sensor pattern. (d) Finally, we subtract this pattern from all the images of the sequence.

Next, we used a robust rigid registration method to stabilize our structures of interest. We propose an adaptive registration, taking as parameter the list of frames, the range of the registration and a binary mask. The range of the registration specifies how long a reference frame is use for. The mask parameter selects a region of interest for registration. To find the transformation, we used a keypoint-based method, that matches keypoints by pairs. Key points were extracted in images using the SIFT method [9]. Point descriptors were matched via brute force and sorted according to their distance coefficient. We kept at most the 10 best pairs of points belonging to the mask. This yields the transform parameters after an iterative RANSAC-like method [10] to weed out the outliers. Due to lack of space, we do not fully develop this method here, however matching pairs rather than individual points allow us to better constrain the result [11]. We also perform model selection, allowing three types of transformations between each pair of frame: identity, pure translation or translation plus rotation. We neglect non-rigid deformations. We choose the best model taking into account both the error and the complexity of the model.

$$P_1 = P_2 \times \mathcal{R} + \mathcal{T} \tag{2}$$

Where P_1 and P_2 are the sets of points of the two frames we seek to match, $\mathcal{R} = \begin{pmatrix} \cos\theta & \sin\theta \\ -\sin\theta & \cos\theta \end{pmatrix}$ is the rotation matrix. $\mathcal{T} = (d_x, d_y)$ is the translation;

$$\forall (x, y) \in I_{clear} : I_{reg}(x, y) = I_{clear}(x', y') \tag{3}$$

with the estimated $\mathcal{R}$ and $\mathcal{T}$, $[x'\ y']^\top = \mathcal{R}[x\ y]^\top + \mathcal{T}$. $\mathcal{S}_3$ is the resulting stabilized sequence of I_{reg}

Then we computed the average image of the sequence (Fig. 2 (b)), yielding an image of the non-moving parts of the sequence. We subtracted this result from each frame. This operation removes the static parts of the sequence and yields only a sequence of moving elements.

$$\forall I_{reg} \in \mathcal{S}_3 : I_{mov} = I_{reg} - \bar{\mathcal{S}}_3 \tag{4}$$

with $[x'\ y']^\top = \mathcal{R}[x\ y]^\top + \mathcal{T}$. $\mathcal{S}_4$ is the sequence of I_{mov}

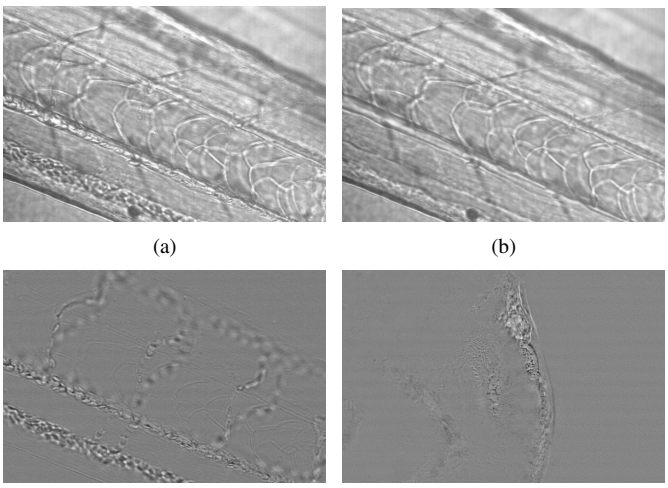

(a) (b) (c) (d)

Fig. 2. Detecting the moving areas of the sequence. (a) Initial frame. (b) Averaging of the sequence yielding the non-moving parts, including all the parts that are not blood cells. (c) Areas with motion from the difference between frames and (b). (d) Equivalent result on a beating heart.

Illumination variations may occur during the sequences. To correct for these, we compute the average value of the sequence, and multiply each pixel by this value divided by

the average of the frame. For each pixel :

$$\forall (x,y) \in I_{mov} : I_{corr}[x,y] = I_{mov}[x,y] \frac{\mu_{\mathcal{S}_4}}{\mu_{I_{mov}}} \tag{5}$$

where $\mu_{\mathcal{S}_4}$ is the average value of the sequence and $\mu_{I_{mov}}$ is the average value of the frame We obtain a sequence S_5 where the average value of all frames is constant throughout the sequence.

C. Segmentation of motion area

At the end of our pipeline, the areas where motion is present are our regions of interest, but each region may not exhibit the same motion everywhere. We segment them according to connectivity criteria, under the assumption that connected parts will exhibit consistent motion (e.g. in a single vessel all blood cells move in the same direction). To achieve this, we integrated the absolute value of the first few frames to obtain an image of the motion areas. Then we computed a labelled mask using a morphological closing and connectivity criteria [12].

$$\textit{sumdiff} = \sum_{i=0}^{10} I^i_{corr} - I^{i+1}_{corr} \tag{6}$$

$$\mathcal{M} = \gamma_{\mathcal{B}_5}(\varphi_{\mathcal{B}_5}((\textit{sumdiff})_{\geq \theta_O})) \tag{7}$$

Where θ_O is the Otsu threshold [13]; $\gamma_{\mathcal{B}_5}$ and $\varphi_{\mathcal{B}_5}$ are respectively the morphological opening and closing [14] by structuring element $\mathcal{B}_5$, a discrete Euclidean ball of radius 5. $\mathcal{M}$ is the mask of the vessels. We created $\mathcal{M}_L$ in which all connected component are distinguished with the attribution of a label. We should expect a maximum number of 2 labels (corresponding to the artery and the vein) for vessels sequences, whereas in heart we should expect a unique label. Figure 3 shows the steps of this segmentation.

III. Results

A. Optical flow

Optical flow is the apparent motion of objects between two consecutive images. We make three assumptions: object pixels intensities do not change between consecutive images; the acquisition rate is sufficiently high to ensure motion is smooth enough for differential calculus to be used, and neighbouring pixels show similar motion.

Because we are working on complex sequences of living models, various frequencies may be present all over the image. A dense optical flow method is preferable when coupled with a labelling of the zones with consistent motion and frequency.

B. Algorithm

We used the Färneback's algorithm for computing the optical flow [15]. It works by dividing the frame with a grid, and calculating global motion in relation to its consecutive frame for each zone. The global motion is assigned to a point representing the center of the zone. For each point we have a displacement vector (see Fig. 4(a,b)). This method is suitable because it is not possible to track individual blood cells in our videos.

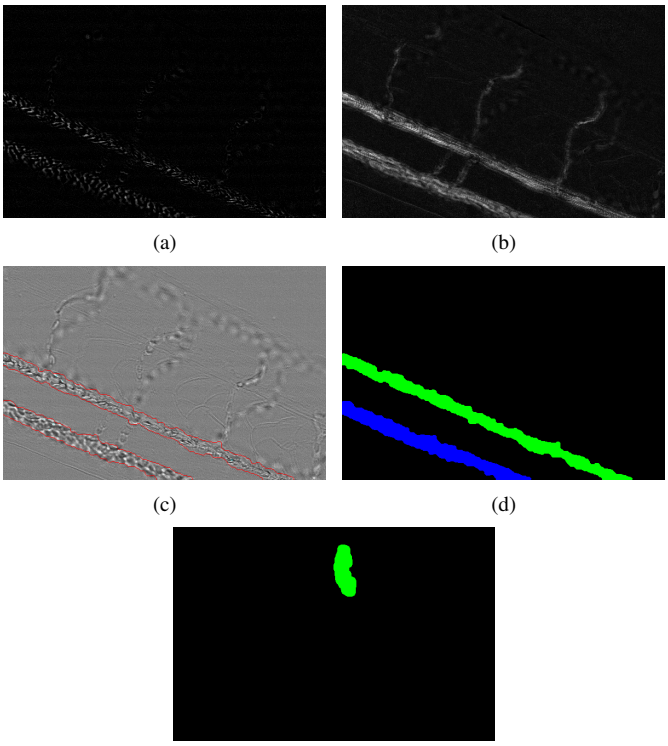

Fig. 3. Sequence of operations for segmentation. (a) Difference between two consecutive frames. (b) Integrating motion yields segmentation (c) and vessel labeling (d). Equivalent labeling in a heart (e): a single area is segmented.

$$V(i) = \bigcup_{\alpha \in M_L} V_\alpha(i) \tag{8}$$

$$\forall \alpha \in M_L, V_\alpha = \{v_i \in V / \mathcal{M}_L(x_{v_i}, y_{v_i}) = \alpha\} \tag{9}$$

$$\mathcal{V}_\alpha(i) = \text{median}(V_\alpha(i)) \tag{10}$$

$V(i)$ is the list of the displacement vectors between two frames $I_{corr}(i), I_{corr}(i+1)$. $V_\alpha(i)$ is the list of the displacement vectors belonging to the component α of M_L. For each region α, we have a median displacement value $\mathcal{V}_\alpha(i)$ which is the global value of displacement in the α region. We validate the choice of the median with speed vector clustering (see Fig. 4(c)).

We identify average motion vectors with each segmented and labelled region. The plot of the magnitude of the speed vs. time in each labelled region allows us to identify useful physiological measurements, such as frequency, minimum and maximum speed, motion regularity and so on. Frequency analysis is performed using the Fast Fourier Transform. These are illustrated in Fig. 5.

C. Speed variations analysis

We can observe two different behaviours in blood vessels: speed profile of veins and arteries are different. We observed wide variations of speed in the arteries while in the veins the speed is almost constant (see Fig. 4(d)). This is to be

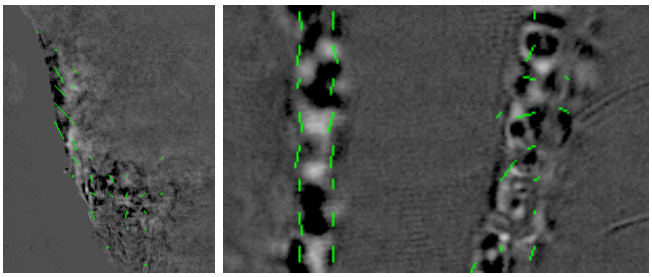

(a) (b)

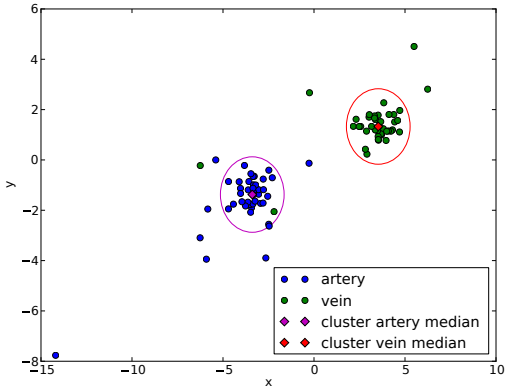

(c)

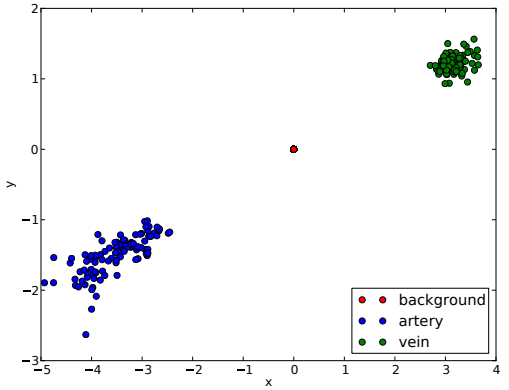

(d)

Fig. 4. Speed analysis on a sequence. Optical flow estimation in a heart (a) and vessel (b). Left vessel is the artery, right is the vein. (c) Speed vector clustering and median values, notice speed consistency in each labeled region. (d) Median speeds during a whole sequence, showing direction and speed variation.

expected since arteries are closer to the ventricular expulsion, whereas veins convey blood that has gone through the whole body and so speed variations are damped. For this reason, we focus only on measurements in arteries to extract physiological parameters such as heart rate.

IV. Validation

Our optical flow-based method can be used to measure speed variations in arteries and around the heart, and so should be correlated with heartbeats. To validate our approach, we first consider frequency estimations in heart sequences. Then

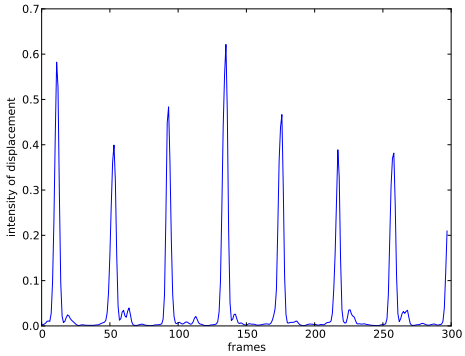

(a)

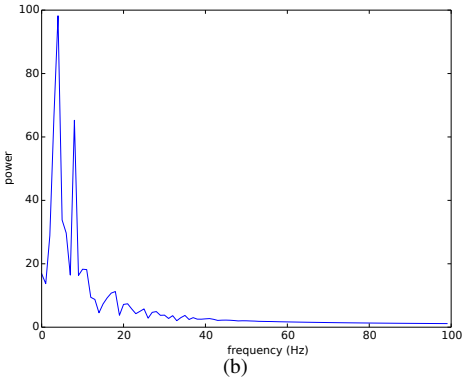

(b)

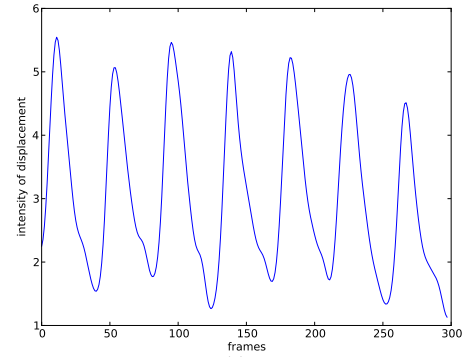

(c)

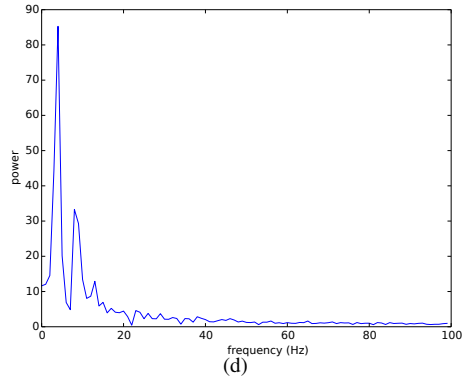

(d)

Fig. 5. Speed frequency analysis on a sequence. Speed variations vs. time over a complete heart sequence (a) and vessel sequence (c). Corresponding Fast Fourier Transform (b) and (d) (cropped to 100 Hz).

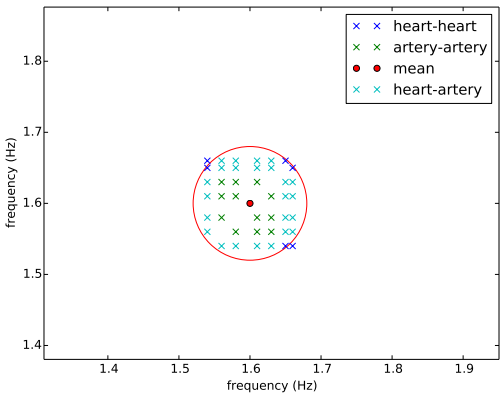

(a)

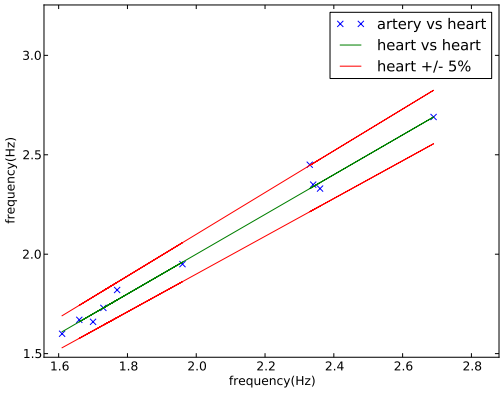

(b)

Fig. 6. Correlation between heart and arteries sequences (a) in a single fish embryo with multiple observations and (b) for 10 subjects exposed to varying environmental conditions.

we compared frequency estimation in vessels with frequency estimation in the heart. Finally, we compare our speed estimations with another method.

A. Manual heart rate validation

For a first validation of our frequency estimation procedures, we first estimated manually the beating frequency in the heart. This is acceptable since the fish embryo heartbeat is easy to follow in the sequence. We recorded several sequences on various embryos (the video acquisition lasted several minutes for each embryo) and we counted the number of heart cycle by watching the sequences at low speed. We compared it with the estimation of our approach. In all the cases, we obtained the same results for both methods up to rounding.

B. Heart vs. vessel validation

To validate our approach in vessels, we estimated heartbeat frequencies in a single fish embryo. Each estimation was performed on 18 different video acquisitions separated by several minutes, and we estimated the frequencies in both the heart and the arteries. Because heart estimation was validated previously, we considered it as our ground truth. In Fig. 6(a), we plotted all possible couples of measurements against each other. All measurements appear consistent and fit within a 5% uncertainty circle, so we can now consider them reliable.

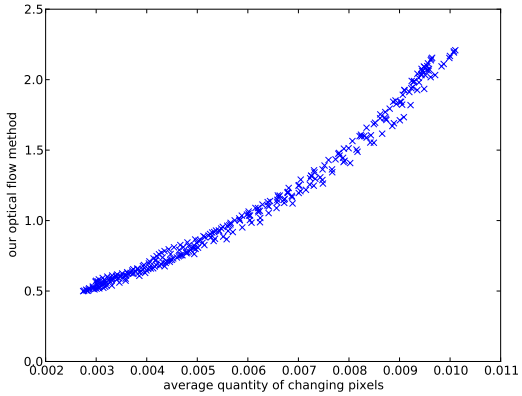

Fig. 7. Comparison with the method of [7] in the ideal single-vessel case.

C. Heart rate variations validation

We also measured the heart rate in the heart and artery in 10 fish embryos subjected to varying environmental conditions, causing the heart rate to vary significantly. We see that our estimations of the heart rate and the frequency measured in the arteries correlate very well as illustrated in Fig. 6(b).

D. Speed measurement validation

Finally we compared our blood cell speed measurement vs. the method of [7]. This latter, simpler method relies on counting changing pixels between frames rather than estimating a flow. It is only reliable in a sequence containing a single vessel, in a noise-free and vibration-free environment. However in this ideal case it is well-correlated, although non-linearly, with ours. The non-linearity in the correlation may be explained because our speed estimate uses a multi-scale approach, whereas [7] is single-scale. Consequently our speed estimates have a wider range (a ratio of 5 vs. 3 between the highest and lowest values). However, reproducibility between cycles is good (see Fig. 7).

V. Conclusions

We have proposed novel ways of estimating frequencies from some cyclic physiological parameters such as heart function and blood flow in arteries in medaka embryo. To achieve this, we have described a complete, versatile, robust pipeline including denoising, sensor grid elimination, stabilization, and optical flow measurement. We have shown that we can successfully estimate frequencies from optical flow speed variations, both around the heart and in blood vessels. The frequencies are consistently estimated and correlate with each other with a low margin of error. This ability to accurately estimate the heart rate from optical flow rather than intensity variations extends the range of possible physiological measurements. Indeed, it is often easier to locate an artery in the tail of a fish embryo than to obtain a clear view of the heart, especially in later stages of development. In future work, we

will study more sophisticated measurements such as estimation of ejection fractions.

REFERENCES

[1] S. L. Oxendine, J. Cowden, D. E. Hinton, and S. Padilla, "Adapting the medaka embryo assay to a high-throughput approach for developmental toxicity testing," *NeuroToxicology*, vol. 27, no. 5, pp. 840–845, Sept. 2006.

[2] D. J. Milan, T. A. Peterson, J. N. Ruskin, R. T. Peterson, and C. A. MacRae, "Drugs that induce repolarization abnormalities cause bradycardia in zebrafish," *Circulation*, vol. 107, pp. 1355–1358, 2003.

[3] G. Paterson, J. M. Ataria, M. E. Hoque, D. C. Burns, and C. D. Metcalfe, "The toxicity of titanium dioxide nanopowder to early life stages of the japanese medaka (oryzias latipes)," *Chemosphere*, vol. 82, pp. 1002–1009, 2011.

[4] A. M. Plotnik and S. M. Rock, "Quantification of cyclic motion of marine animals from computer vision," in *MTS/IEEE OCEANS'02*, 2002, vol. 3, pp. 1575–1581.

[5] Dongmin G., A. L. van de Ven, and Xiaobo Z., "Red blood cell tracking using optical flow methods," *IEEE Journal of Biomedical and Health Informatics*, vol. 18, no. 3, pp. 991–998, May 2014.

[6] RT Doyle, T Moninger, N Debavalya, and WH Hsu, "Use of confocal linescan to document ciliary beat frequency," *Journal of Microscopy*, vol. 223, pp. 159–164, 2006.

[7] S.H. Cheng and P.K. CHAN, "Method of in vivo screening for cardiac toxic agents using teleost," Sept. 17 2009, US Patent App. 12/224,577.

[8] B. K. Horn and B. G. Schunck, "Determining optical flow," in *1981 Technical Symposium East*. International Society for Optics and Photonics, 1981, pp. 319–331.

[9] D G Lowe, "Object recognition from local scale-invariant features," in *IEEE International Conference on Computer Vision*, Kerkyra, Greece, September 1999, vol. 2, pp. 1150–1157.

[10] M. A Fischler and R. C Bolles, "Random sample consensus: a paradigm for model fitting with applications to image analysis and automated cartography," *Communications of the ACM*, vol. 24, no. 6, pp. 381–395, 1981.

[11] T. Collins, P. Mesejo, and A. Bartoli, "An analysis of errors in graph-based keypoint matching and proposed solutions," in *European Conference on Computer Vision*, Zurich, Switzerland, September 2014, vol. 8695 of *LNCS*, pp. 138–153, Springer.

[12] L. Najman and H. Talbot, Eds., *Mathematical Morphology: from theory to applications*, ISTE-Wiley, London, UK, September 2010, ISBN 978-1848212152.

[13] N. Otsu, "A threshold selection method from gray-level histograms," *Automatica*, vol. 11, no. 285-296, pp. 23–27, 1975.

[14] H. Heijmans, *Morphological image operators*, Advances in Electronics and Electron Physics Series. Academic Press, Boston, 1994.

[15] G. Farnebäck, *Polynomial Expansion for Orientation and Motion Estimation*, Ph.D. thesis, Linköping, 2002.